2017

# Design and Verification of a Multi-Terawatt Ti-Sapphire Femtosecond Laser System

Patrick Roumayah
*University of Central Florida*

# DESIGN AND VERIFICATION OF A MULTI-TERAWATT TI-SAPPHIRE FEMTOSECOND LASER SYSTEM

by
PATRICK ROUMAYAH
B.S. University of Michigan, 2011

A thesis submitted in partial fulfillment of the requirements
for the degree of Master of Science
in the College of Optics and Photonics
at the University of Central Florida
Orlando, Florida

Spring Term
2017

Major Professor: Martin Richardson

# ABSTRACT

Ultrashort pulse lasers are well-established in the scientific community due to the wide range of applications facilitated by their extreme intensities and broad bandwidth capabilities. This thesis will primarily present the design for the Mobile Ultrafast High Energy Laser Facility (MU-HELF) for use in outdoor atmospheric propagation experiments under development at the Laser Plasma Laboratory at UCF. The system is a 100fs 500 mJ Ti-Sapphire Chirped-Pulse Amplification (CPA) laser, operating at 10 Hz. Some background on the generation of very high intensity optical pulses is also presented, alongside an overview of the physics of filamentation.

As part of the design of MU-HELF, this thesis focuses on a novel approach to manage the large amount of dispersion required to stretch the pulse for CPA utilizing a custom nonlinear chirped Volume Bragg Grating (VBG) as a pulse stretcher matched to a traditional Treacy compressor. As part of this thesis, the dispersion of the CPA system was thoroughly modeled to properly design the chirped VBG and fabricated VBGs were characterized using a scanning spectral interferometry technique. The work demonstrates the feasibility of using a compact monolithic pulse stretcher in terawatt class CPA lasers.

# TABLE OF CONTENTS

# LIST OF FIGURES

# INTRODUCTION AND MOTIVATION

The Laser Plasma Laboratory at CREOL is developing an ultrashort pulse near-IR laser for use in field propagation studies, including the creation and study of very long filaments[1]. Applications for such lasers include but are not limited to remote supercontinuum sensing, plasma channel electric discharge guidance (laser induced lightning), and laser induced plasma x-ray sources[2, 3]. There has been research into missile countermeasure applications, and promising results using the high intensity pulses to damage guiding optics[4].

The Mobile Ultrafast High Energy Laser Facility (MU-HELF) will include a self-contained, sub ps, 500 mJ, 780 nm pulsed laser system specifically designed for stability and usability in a variety of climates and environments. The container is a 40 ft shipping container, and provides a control room, gowning area, and clean room to house the laser itself, as well as the Laser Optics Turret and Instrumentation System (LOTIS) laser tracking mount. The LOTIS is an active beam tracking and directing system with up to 190 nrad resolution in lab conditions and is the first dynamic tracking system to be used with targets over a very large field of view illuminated by an ultrashort pulse laser system over multi kilometer ranges.

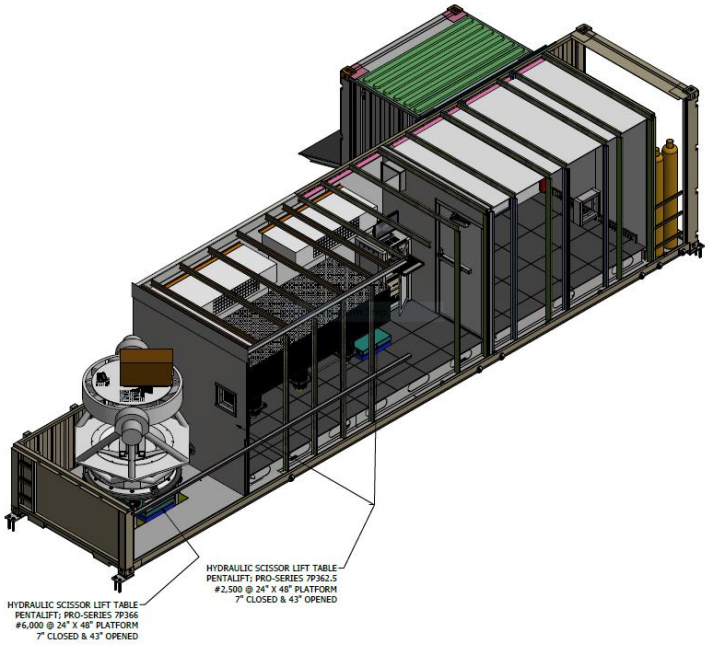


Figure 1. 3-dimensional schematic of the MU-HELF

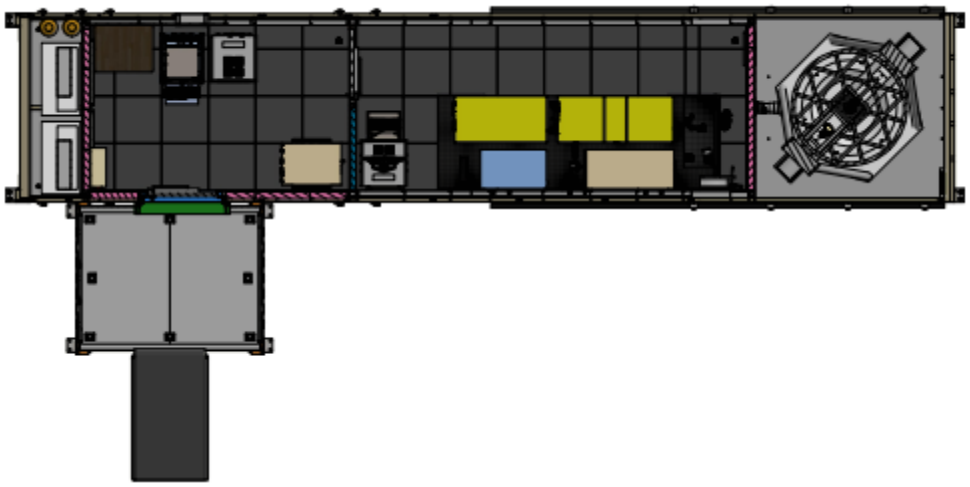

Figure 2. Floorplan of the MU-HELF.

The MU-HELF improves over previous mobile short-pulse lasers, such as the TeraMobile[5] in several ways. We anticipate greater energy per pulse: 500 mJ vs 350 mJ, the MU-HELF can extend the filamentation process further, or produce more filaments. It has greater stability thanks to a fiber oscillator rather than a solid state Ti-Sapphire oscillator and a stretcher that uses a solid state chirped Volume Bragg Grating (VBG) pulse stretcher, rather than a diffractive grating pair. This front end also allows for a smaller footprint which is crucial in a self-contained mobile laser system, where space is very limited.

LPL has long experience in femtosecond NIR laser systems. The Multi-Terawatt Filamentation Laser (MTFL) facility: a 300 mJ class 40 fs laser system and the High Energy, Repetition rate Adjustable, Carrier Locked to Envelope System (HERACLES): a few fs optical parametric chirped pulse amplification laser are both ultrashort pulse laser facilities in operation under the LPL. The experience gained from experiments in MTFL and HERACLES has led to several important insights about the importance of measurements and stability in an ultra-short laser system. The diagnostic techniques developed in MTFL have been applied in MU-HELF to maximize performance and stability while minimizing downtime for realignment and troubleshooting.

# ULTRASHORT LASER SOURCES

Ultrashort laser systems demand management of bandwidth and dispersion, avoiding optical damage associated with very high fluence and intensities, and precise measurement[6]. This section will offer some background in short pulse, high energy laser sources in general, as well as the specific methods employed in the MU-HELF system.

## Short Pulse Generation

While discussing short pulse generation, it is important to discuss some terms. "Bandwidth" refers to the constituent frequencies of a light pulse; the shorter a pulse, the larger the bandwidth required to produce it. The transform limit is the shortest possible pulse duration for a given bandwidth and is achieved when all of the constituent frequencies are in phase with each other. For Gaussian pulse shapes,

$$\tau_{p\,(TL)} = \frac{2*\pi}{2\omega_b} \quad [7] \qquad (1)$$

Where $\tau_{p\,(TL)}$ is the transform limited pulse duration and $\omega_b$ is the frequency bandwidth. This relation holds true for Gaussian pulse duration and spectral content, and is sufficiently accurate to describe the spectra exhibited by the MU-HELF system.

There are several methods for generating very short pulses: Q switching, gain switching, and mode locking will all be discussed here, with an emphasis on mode locking.

## Q switching

Active Q switching is the process of quickly varying cavity losses (usually by way of an acousto-optic modulator, electro-optic modulator, or piezo resistor) in order to output energy stored in the gain medium in a short pulse on the order of ns. Effectively, the energy is stored in the "off" condition while the cavity Q is low. The inversion of the gain medium increases to much higher than in CW, when the cavity Q is increased a pulse rapidly builds up from noise and extracts the stored energy [8-10].

Figure 3 demonstrates an active Q switched pulse on the order of 500 ns, and the corresponding function generator output to an intracavity AOM. While the AOM is on, light is deflected, "turning off" the cavity. Note, the AOM is turned off for a brief time, lowering the loss in the cavity, which allows for the stored energy to be output.

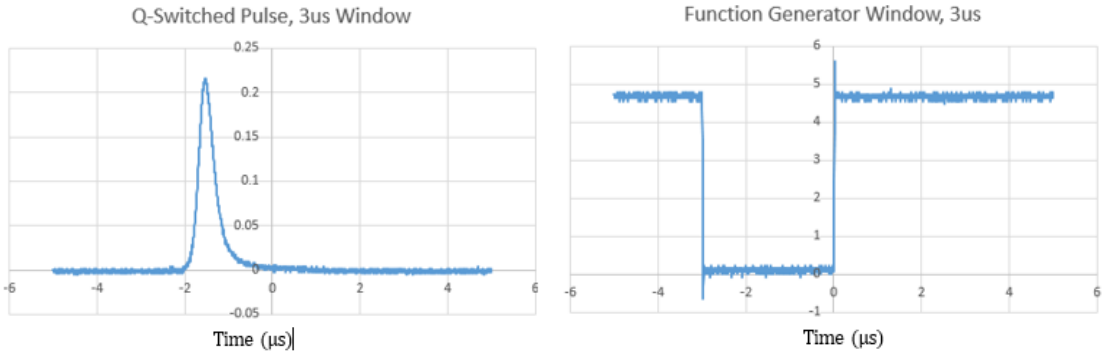


Figure 3. Example of a Q switched pulse.

## Gain Switching

Gain switching functions under a similar principle, but the gain is modulated (by modulating the pump power) rather than the loss in the cavity. The pump power is kept at a level below the lasing threshold, then suddenly increased to above the lasing threshold. In the CW case, the inversion oscillates and relaxes to the steady-state value; in gain switching the pump can be modulated to release as little as a single relaxation oscillation with a high peak power [11, 12].

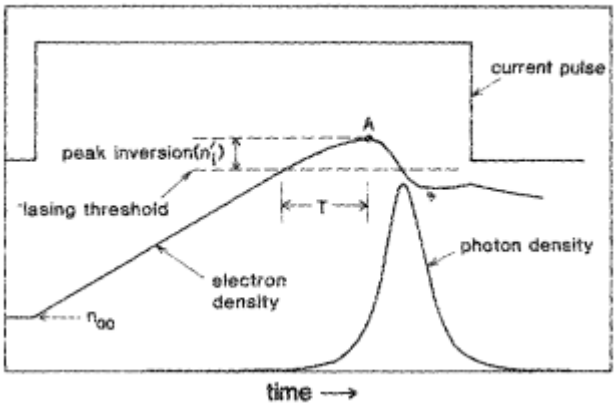


Figure 4. Schematic of gain switched pulse [12].

## Mode Locking

Theorized and reported soon after the advent of the laser [13, 14], active mode locked lasers use some modulation technique like active Q switched lasers, but they modulate at a resonant frequency related to the free spectral range of the laser cavity: the difference between the frequencies of allowable longitudinal modes.

$$v_{fsr} = \frac{c}{L * n_g} \quad [7] \qquad (2)$$

In equation 2, $v_{fsr}$ is the free spectral range, c is the speed of light, L is the round trip path of the cavity, and $n_g$ is the refractive index in the optical path. This modulation generates sidebands in the frequency space of the gain medium that match other supported longitudinal cavity modes. As the supported cavity modes are all separated by the free spectral range, the effect repeats until the entire gain bandwidth is filled; all possible longitudinal modes are amplified, rather than only one near the gain peak. This produces a very large bandwidth and a very short pulse. It is important to note that without dispersion management, dispersion typically limits the mode locked bandwidth to smaller than the bandwidth of the gain medium.

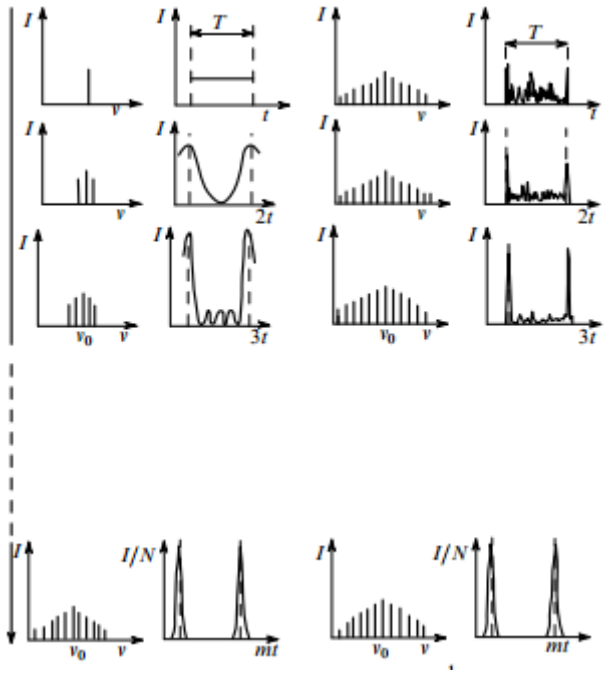


Figure 5. Pulse development of a mode locked laser[6].

Passive mode locking produces short pulses using a very fast saturable absorber: a saturable absorber that can "reset" faster than a round trip of the cavity; and was explored several years after the active configuration[15, 16]. A short circulating pulse becomes the only allowable mode in the laser cavity, as the absorber will suppress lower power modes. Similar to active mode locking, this induces a modulation with a period equal to the round trip time of the cavity; the opacity of the absorber is lowered while it is sees the circulating pulse each round trip. This is the most common method for pulse generation for femtosecond lasers, and is the principle behind both the Ti-Sapphire oscillator in the laser plasma laboratory's MTFL laser and the Erbium fiber oscillator in the MU-HELF system. Once the pulse is generated by the oscillator, it is amplified to much higher energies through Chirped Pulse Amplification (CPA).

## Chirped Pulse Amplification

CPA is a method for amplifying short pulses to very high powers, first explored in the mid-1980s[17, 18]. For example, it is not possible to directly amplify a 100 fs pulse beyond mJ energies without inducing undesirable nonlinear effects and/or optical damage. CPA avoids this limitation, by engineering the dispersion of the system such that the nearly transform limited pulse (100 fs for MU-HEL) is stretched in time. This stretch is accomplished by delaying some frequencies more than others, to broaden the pulse duration and significantly lower peak power while maintaining pulse energy. This change in phase for different frequencies is known as dispersion or chirp.

The chirped pulse is amplified in one or more stages, reaching up to several hundred mJ pulse energy. As the energy is increased, the beam size must be increased as well in order to avoid exceeding the damage threshold fluence[19].

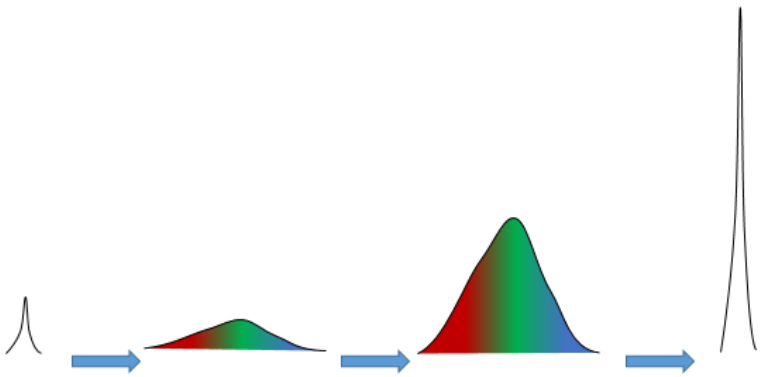

Figure 6. Chirped Pulse Amplification

The dispersion input by the stretcher and the relatively small dispersion of the amplification components must be compensated precisely by the compressor, though most tools have limitations on the shape of the curve of dispersion they can provide. Normally, in order to be able to analyze the full system's and the individual components' dispersion meaningfully, we inspect the Taylor expansion of the phase delay about the center wavelength, and compensate each order individually. This is important, because there are usually some constraints on our control of dispersion; for example, the Treacy compressor we use in our configuration has a set ratio of $2^{nd}$ order to $3^{rd}$ order dispersion. A custom chirped volume Bragg grating or fiber Bragg grating may offer more degrees of control, but sacrifice some precision. The DAZZLER, a programmable dispersive device, offers

more degrees of control, capable of generating a loosely constrained chirp function over several orders[20, 21]. We use all of these components to manufacture and then compensate the chirp, before and after amplification; the specifics of each will be detailed in the following section.

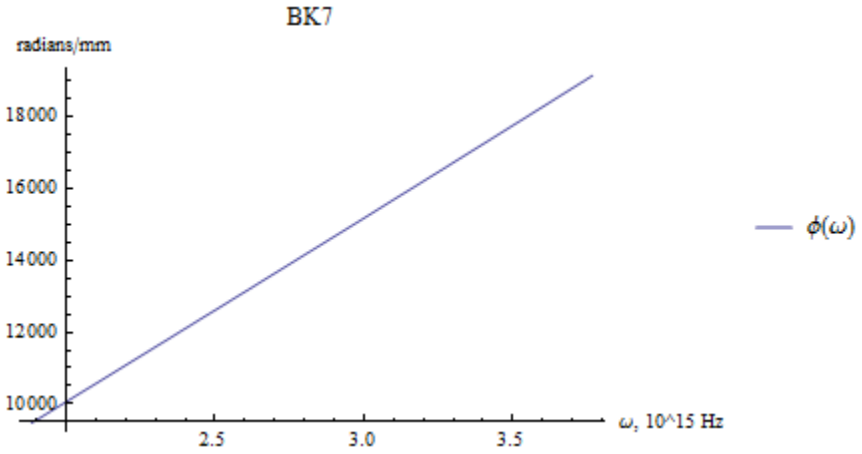


Figure 7. Phase delay of BK7

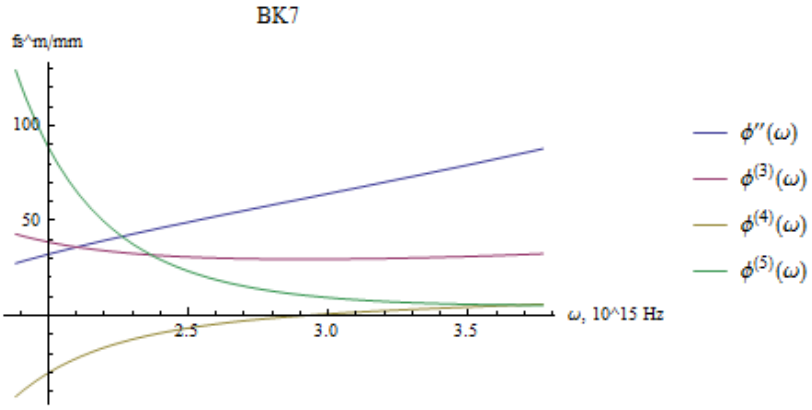


Figure 8. Dispersion of BK7.

Figures 7 and 8 show the phase delay of BK7 and 2nd through 5th order dispersion, in fs^M/mm, as calculated using the Sellmeier equations[22, 23]. These values are calculated for all the constituent materials of the MU-HELF system, and used for the design specifications of the stretcher and compressor.

One unique aspect of the MU-HELF system is the asymmetry of the chirp components; most CPA systems use a similar components for stretching and compressing the pulse. We are using a custom chirped volume Bragg grating to stretch the pulse, to reduce size and potential for misalignment. Large aperture diffraction gratings are required in the compressor in order to handle the TW peak power output. The compressor offers some degree of control to adjust/optimize the overall dispersion of the system, with the DAZZLER for fine tuning.

## Filamentation

Ultrashort light pulses with a duration on the order of femtoseconds ($10^{-15}$ seconds) are critical in a wide range of scientific investigations. The ultrashort pulse duration allows for extremely high power and intensity, which lends itself to studying nonlinear processes including multiphoton absorption, self-phase modulation, Kerr self-focusing, etc. High energy ultrashort pulse lasers also have applications in ablation manufacturing, atmospheric sensing, and are being explored for use in nuclear fusion [24, 25]. The primary application of the MU-HELF laser system is the study of

kilometer range atmospheric propagation of high energy pulses undergoing filamentation, the physics of which are described briefly below.

Filamentation is an example of a spatial soliton (a light beam whose spatial characteristics are unchanging during propagation) arises from a balance between the diverging effects (linear divergence, plasma refraction) and self-focusing [1]. Pulses with very high peak power, greater than the critical value given by equation 3 will self-focus enough to overcome diffraction. [26]

$$P_{crit} = 0.148 * \frac{\lambda^2}{n * n_2} \quad (3)$$

If the induced Kerr lens overcomes beam divergence, the beam will collapse [27]. It is important to note that the critical power does not depend on beam size, which may be unintuitive; though larger diameter beams are less affected by the nonlinear effects of the medium, they are more greatly affected by the effective difference in refractive index. The beam is constrained over some distance determined by the geometrical focus of the system and the self-focusing $n_2$ effects.

The second critical component for filamentation is the formation of a plasma once the intensity of the beam surpasses the ionization threshold. The formation of a plasma (photo-ionization) due to multi-photon absorption and tunnel ionization is strongly dependent on field intensity [28], and occurs suddenly near the beam collapse. The plasma causes a local reduction in refractive index according to equation 4.

$$n \cong n_0 - \frac{\rho(r,t)}{2\rho_c} \qquad (4)$$

Where $\rho$ is the density of free electrons and $\rho_c$ is the value of critical plasma density above which the plasma becomes opaque. This will add to diffraction in order to expand the beam, balancing the effects of self-focusing [27].

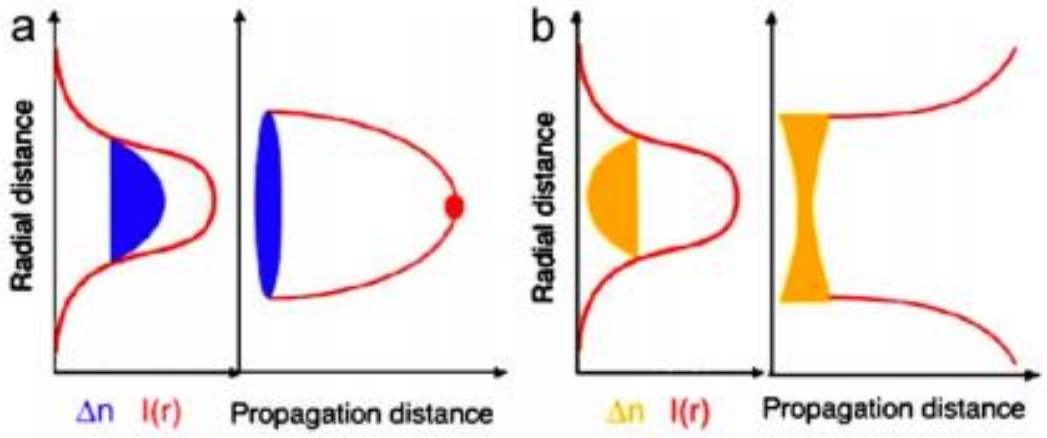


Figure 9. Simple model for self-focusing and plasma defocusing.

In the absence of other nonlinear effects, the high intensity of the laser beam creates a local increase in refractive index (a) that acts as a positive lens, and leads to eventual collapse. When the intensity of the beam is sufficient to cause photo-ionization, the local decrease in refractive index from the plasma acts as a negative lens (b).

The intensity eventually overcomes the ionization threshold, and the plasma divergence effects balance the focusing effects, locking the intensity near the ionization threshold [2]. Below is the

simulated intensity vs distance in vacuum (dashed) and air (solid). Without the second order nonlinearities of air, intensity decreases gradually with distance. With the Kerr self-focusing effects of air, the intensity is locked near the ionization intensity of air [2].

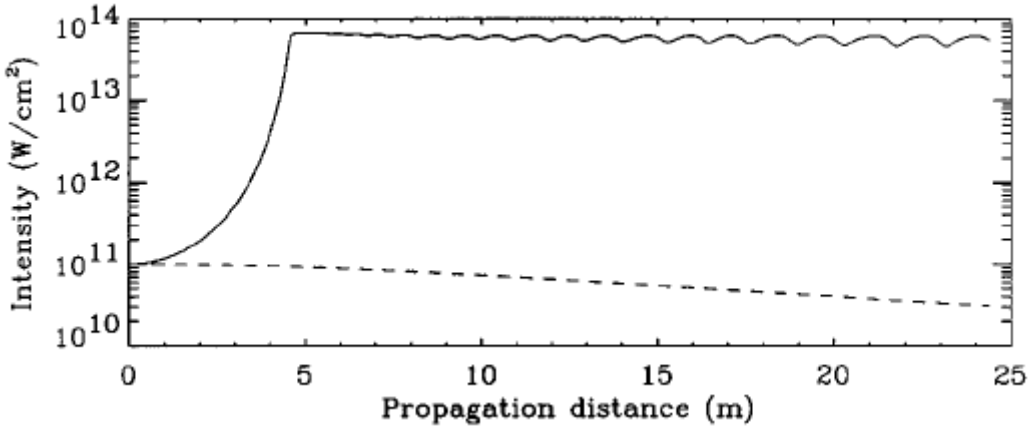


Figure 10. Intensity clamping due to filamentation.

Because the self-focusing, the formation of plasma, and the plasma divergence are functionally dependent on the spatial intensity distribution of the beam, a relatively smooth and temporally stable pulse profile is desirable for single filament experiments, or for well controlled multiple filament arrays. Intensity clamping forms an upper limit to the intensity of the beam; in cases of imperfect or modulated beam profiles, multiple filamentation will occur with sufficient peak

powers. In the case of very smooth beam profiles, the volume of the plasma will increase, while the intensity will remain clamped near the ionization intensity[29].

For applications requiring filamentation at long range, experimentalists use a combination of very long geometric focus, variable initial beam diameter, and chirp[30]. Equation 5 gives filamentation onset distance $z_f$ as a function of initial peak power P, critical power $P_{cr}$, wave vector k, and initial $e^{-1}$ beam radius a. Equation 6 gives $z_f$', the filamentation onset with external focusing.

$$z_f = \frac{0.367ka^2}{\left(\left(\left(\frac{P}{P_{cr}}\right)^{\frac{1}{2}} - 0.852\right)^2 - .0219\right)^{\frac{1}{2}}} \quad (5)$$

$$z_f' = \frac{z_f f_{eff}}{z_f + f_{eff}} \quad (6)$$

Where $f_{eff}$ is the effective focal length of the optical system. Even at a kilometer, the dispersion of air is small compared to the chirp of the laser pulse, but is used to lower the initial peak intensity to postpone plasma formation.[5, 27, 30, 31].

# ARCHITECTURE AND DESIGN

The Mobile Ultrafast High Energy Laser Facility (MU-HELF) includes a chirped pulse amplification laser. It consists of a femtosecond Erbium fiber oscillator emitting at 785 nm, a custom volume Bragg grating, a Ti-Sapphire regenerative amplifier, 2 multi-pass amplifiers, a Treacy compressor made up of two double passed diffraction gratings, and a DAZZLER for precise dispersion control. This section will describe the functionality and physics behind each component in detail, as well as provide the design considerations that have led to this final configuration.

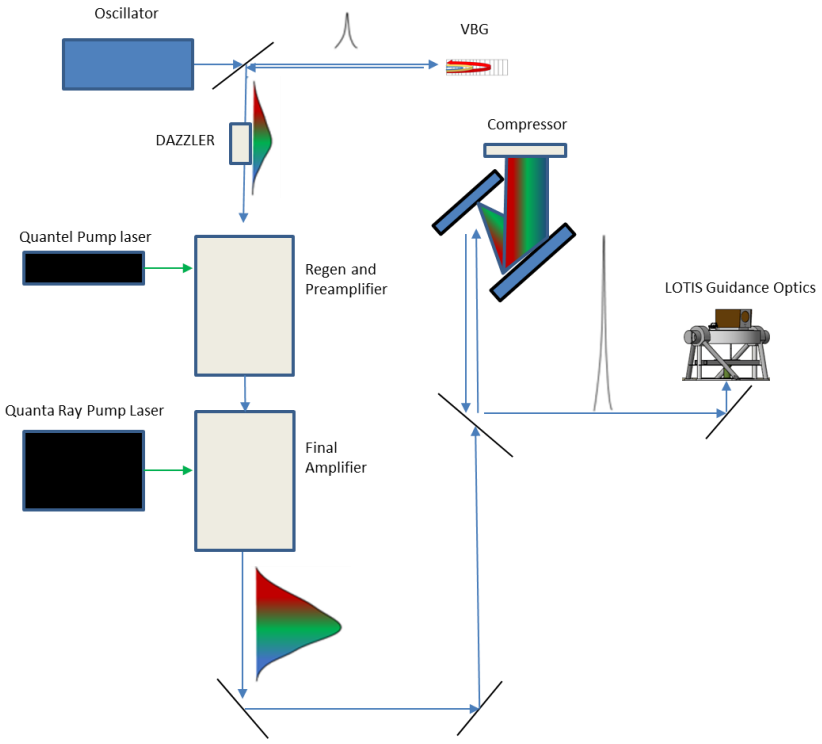


Figure 11. Optical Schematic of the MU-HELF Laser

## Oscillator

The oscillator that produces the seed for the system is a 50mW average power 100fs erbium fiber laser by Toptica (FemtoFErb 780). A passively mode locked fiber laser[32] that uses a semiconductor saturable absorbing mirror (SESAM) to mode lock around 1550 nm. The output is subsequently frequency doubled in periodically-poled lithium niobate (PPLN) to convert the wavelength to 785 nm, within the gain band of Ti-Sapphire. It offers several advantages over solid-state Ti-Sapphire oscillators.

Relative to conventional Ti-sapphire oscillators, the integrated fiber design makes it very stable and "turn-key". Furthermore; the FemtoFErb 780 is very compact, taking up only 69 x 122 x 202 mm. Its electrical power requirement is less than 20W, which becomes important in a mobile system, as power and cooling are both at a premium. It generates 100 fs pulses at 100 MHz at 785 nm with a Gaussian output beam with an $R^2$ of 0.99994. The measured spectrum yields a transform limit of very near 90 fs FWHM with approximately 12 nm FWHM bandwidth.

## Volume Bragg Grating pulse stretcher

The second component in the system is a custom inscribed chirped VBG, to introduce the specific amount of second and third order dispersion required to compensate the rest of the system and the compressor. The technology is based on aperiodic refractive index perturbations, and has been well established for use in dispersion compensation [33, 34]. The Bragg structure is engineered such that different wavelengths reflect at different positions along the volume enabling

customization of the spectral phase over a set spectral bandwidth. The VBG is designed and fabricated by OptiGrate to provide second and third order dispersion of the system derived as part of this masters' thesis [35].

Though chirped VBGs have been available commercially since 2014, nonlinearly chirped volume Bragg Gratings (Gratings with nonzero third order dispersion) are novel and this work is the first time a CVBG has been used to compensate a Treacy compressor. While it is relatively common to use a pair of linear CVBG's in low energy systems, the very high energy output we are expecting from our system prohibits this approach. As the VBG in our setup is only 5mm square aperture, the intensity of the compressed pulse would be many orders of magnitude above the damage threshold. Record pulse compression in VBGs in the fs regime is on the order of 1 mJ [35].

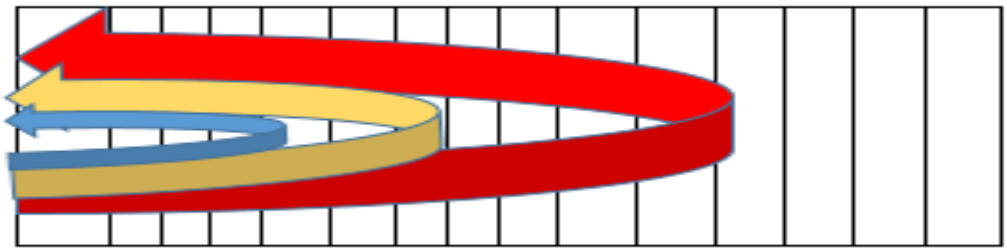

Figure 12. Chirped Volume Bragg Grating.

## Titanium-Sapphire Amplifiers

Titanium-Sapphire has been known as desirable gain medium for very short pulse lasers since the mid-1980s due to its extremely large output wavelength range. The $Ti^{3+}$ is a Vibronic ion, meaning the emission of photons is accompanied by phonons due to lattice vibrations to such an extent as to allow tunability over a very broad range; in the case of a mode-locked laser or a short pulse amplifier, it allows a very broad bandwidth emission and amplification[36].

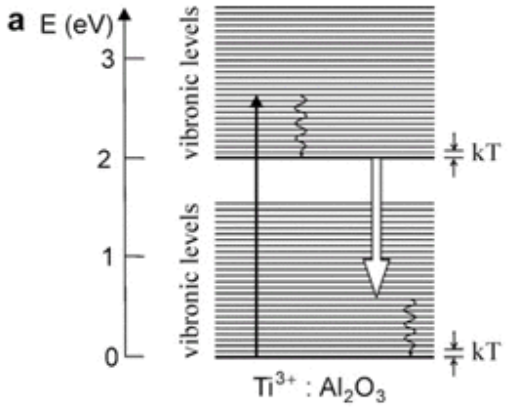


Figure 13. Vibronic energy level diagram of Ti: $Al_2O_3$. [36]

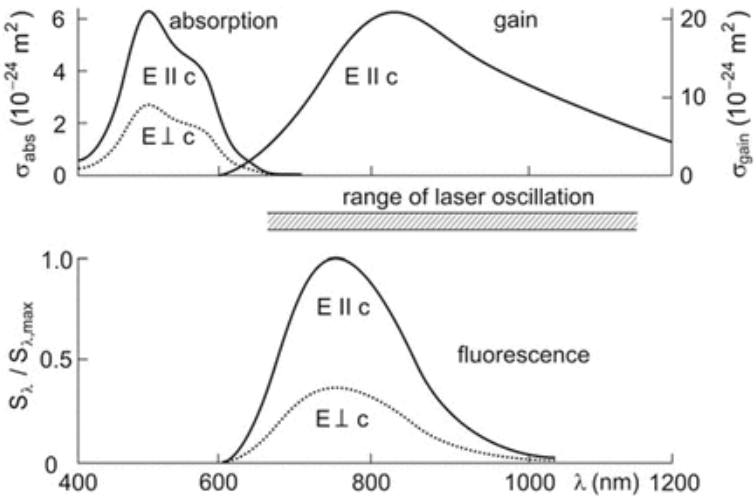


Figure 14. Absorption, Gain, and Fluoresence spectra of Ti: $Al_2O_3$.[36]

This has lead to lasers with outputs as low as 5 fs (with intracavity dispersion correcting elements) Ti-Sapphire is also the primary pumped used for high harmonic generation for Attosecond science. [37]. The MU-HELF will have 20 nm bandwidth (full width half maximum), centered about 785 nm, to support 100 fs time-bandwidth limited pulses. This system uses 3 amplifiers Ti-Sapphire: a regenerative 12-15 pass amplifier, a six pass pre-amplifier, and a 4 pass final amplifier. The regenerative amplifier and the pre-amplifier are pumped at 532 nm from a Quantel green laser,

and the final amplifier is pumped by a Quanta-Ray pro 350; both are 532nm frequency doubled Nd:YAG flashlamp pumped lasers.[27]

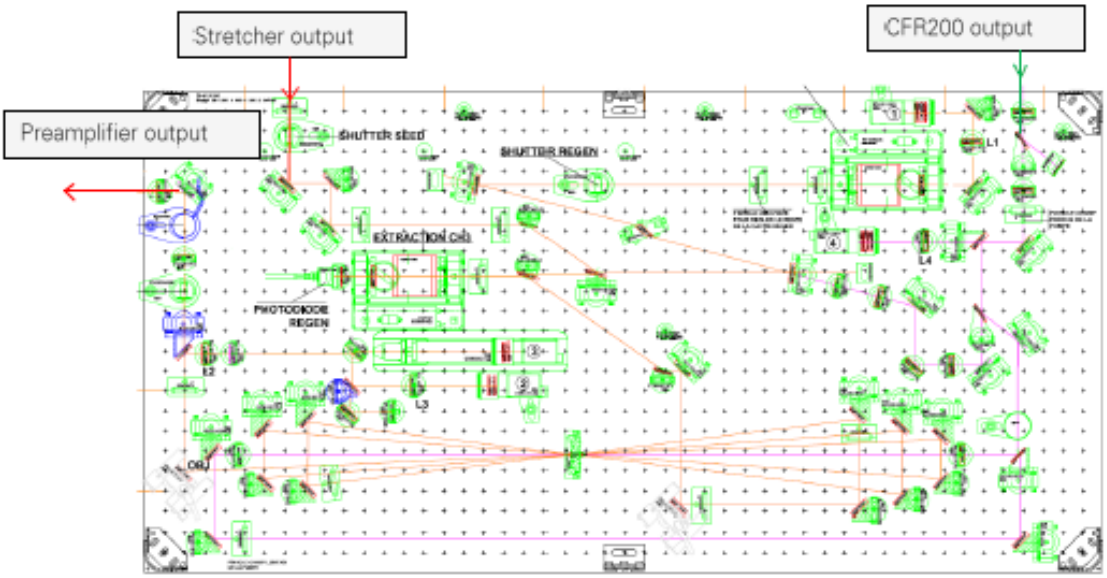


Figure 15. Regenerative Amplifier and Preamplifier

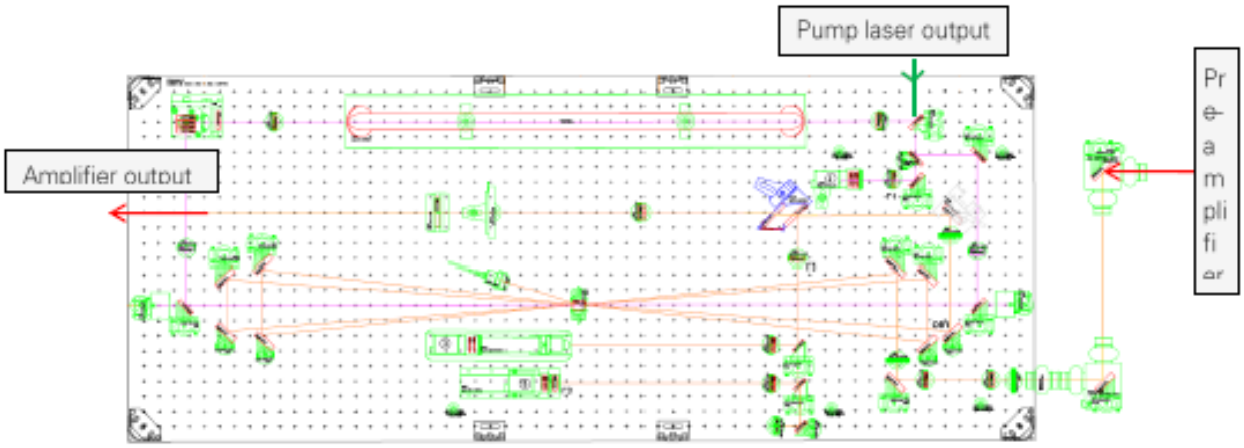


Figure 16. Final Amplifier

## DAZZLER

The DAZZLER is an acousto-optic programmable dispersive filter (AOPDF) that enables customization of the spectral phase over a small range. Acousto-optic modulators function using the stress dependent refractive index of certain crystals in order to form a periodic refractive index "grating" from the compression caused by a sound wave[38]. The DAZZLER by Fastlite modulates the sound wave passed into the crystal, which gives precise control over the phase and amplitude characteristics of the refracted beam[20, 21, 39]. Different frequencies can be refracted at different points along the crystal generating spectral chirp, and modulation depth can be varied to control the amplitude of the pulse.

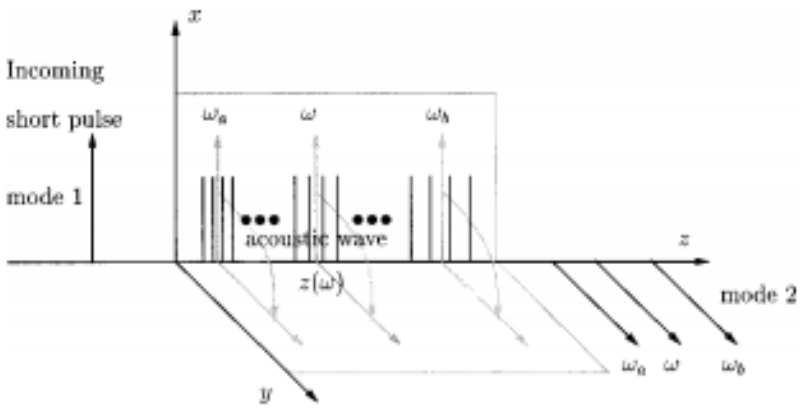


Figure 17. Functional description of the AOPDF [20].

**Treacy Compressor**

Reflective gratings function by reflecting different wavelengths at different angles, introducing spatial chirp. As first demonstrated by Treacy, 2 parallel gratings can be arranged such that the optical path length is a function of the wavelength. The beam is then reflected off of a periscope, back onto the second grating and again onto the first, such that the difference in optical path length becomes the induced dispersion. In a Treacy compressor, 2nd and 3rd orders of dispersion dominate [40].

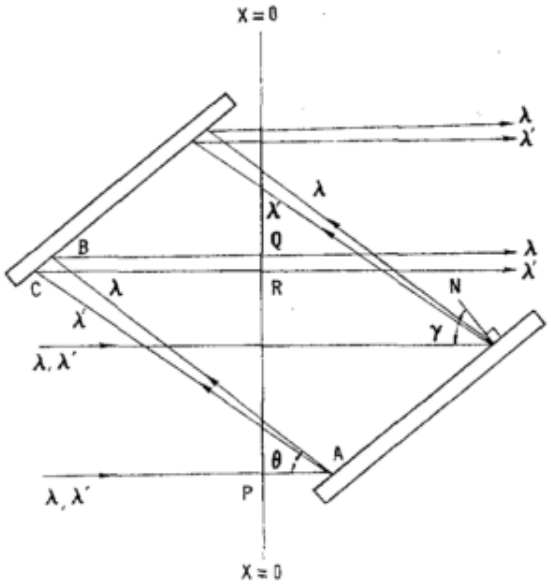


Figure 18. Treacy Compressor [40].

# DISPERSION AND STABILITY

The most important attribute of an ultra-short pulse laser for use in a mobile system is stability, as it will be subjected to stressful environments including a relatively wide variety of temperatures and humidity beyond the norm for a laboratory based laser. The trailer and enclosure will compensate for large scale environmental variation, but from experience with static femtosecond laser systems it is known that temperature variation in the regenerative amplifier, as small as 0.2° C, can have detrimental effects on the pulse duration and amplitude by affecting the pointing vector. In this section, we define the methods used for dispersion compensation and explore how instability in temperature and humidity might affect peak power.

## Nominal Dispersion

Without an adjustable grating system for the pulse stretcher, it becomes extremely important to have a very accurate estimation of the system dispersion.

While the custom dispersion optics are only tunable to the $3^{rd}$ order, the rest of the system dispersion was approximated to at least the fourth order by way of measuring material thickness, and finding the unitary dispersion for each order and material. To this end, we perform a differentiation of the phase $\varphi(\omega)$ using the Sellmeier equation to approximate the refractive index n (note, this assumes that R, an arbitrary vector through the optical system is collinear with k, the propagation vector).

$$\varphi(\omega) = k(\omega) \cdot R = \frac{\omega * n(\omega) * R}{c} \quad (7)$$

The first derivative, is tied to "group delay" $\tau_g$ which does not affect to pulse duration.

$$\tau_g = -\varphi'(\omega). \quad (8)$$

The second derivative of the total phase accumulated per angular frequency is the group delay dispersion, which is related to linear chirp and used to "stretch" or "compress" the pulse duration. Higher orders of chirp (higher derivatives of phase accumulation) also have an effect on pulse shape and duration, and may need to be compensated. In our system, we will rely on the DAZZLER to compensate dispersion above the 3rd order, but it is important to have an accurate model of these higher orders to know how much and of which sign of dispersion to program into the DAZZLER. The materials include BK7, fused silica, Ti:sapphire, KDP, air, the acousto-optical crystal that makes up the DAZZLER, the VBG stretcher, and the Treacy compressor.

The nominal dispersion of the system can be optimized by mechanical optimization of the Treacy compressor to at least 88% of the transform limited peak power. The DAZZLER allows for fine dispersion compensation up to very near the transform limit.

The optimization of the compressor will be slightly different from design parameters due to the precision of the VBG. To demonstrate the sensitivity of the Treacy compressor, we compare the

design of 32° incident angle into the first grating, and longitudinal separation of 28.66 cm with optimization was found at 31.86° and 28.16 cm.

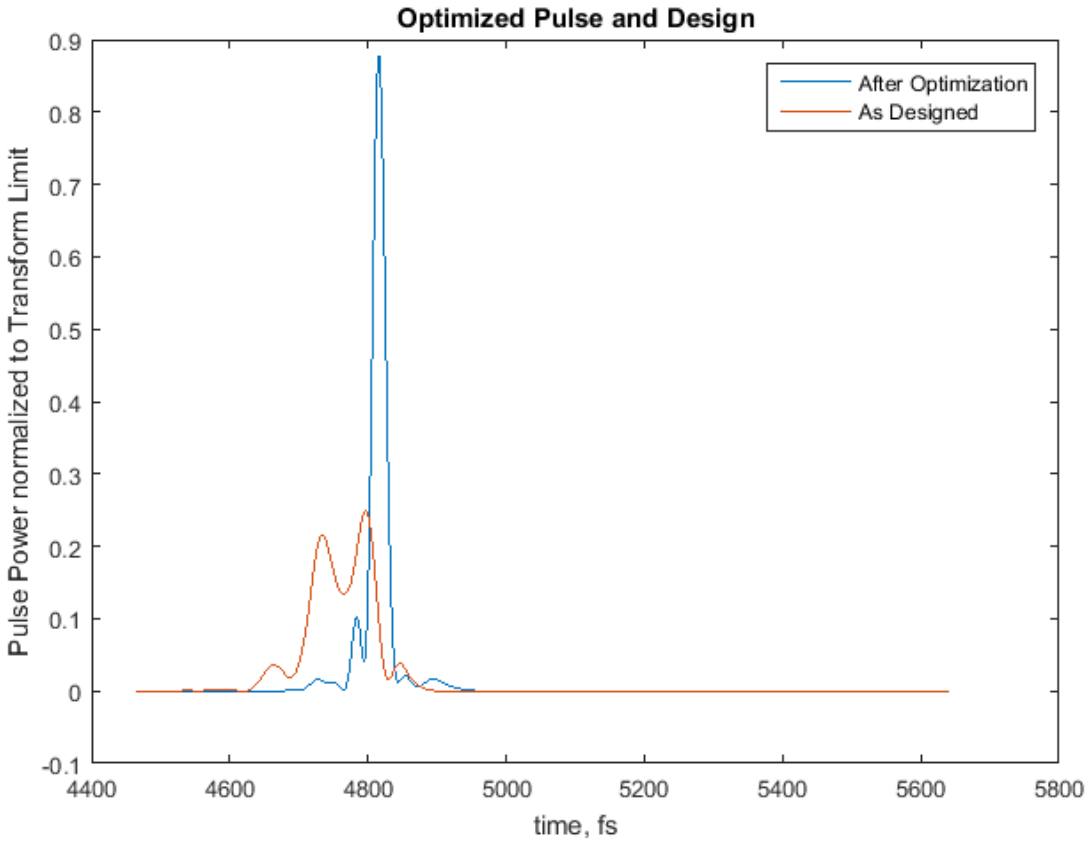


Figure 19. Variation of pulse envelope between design parameters and numerical optimization.

## Stability

It is important to all ultra-short pulse lasers that the temperature, humidity, and mechanical stability be maintained. To give approximate worst-case analysis of variation of temperature and humidity,

the dispersion variation due to refractive index changes over temperature, and over variation in angle and grating separation were simulated. We find that refractive index of air does not alter our dispersion significantly (for temperature fluctuations of 20°C).

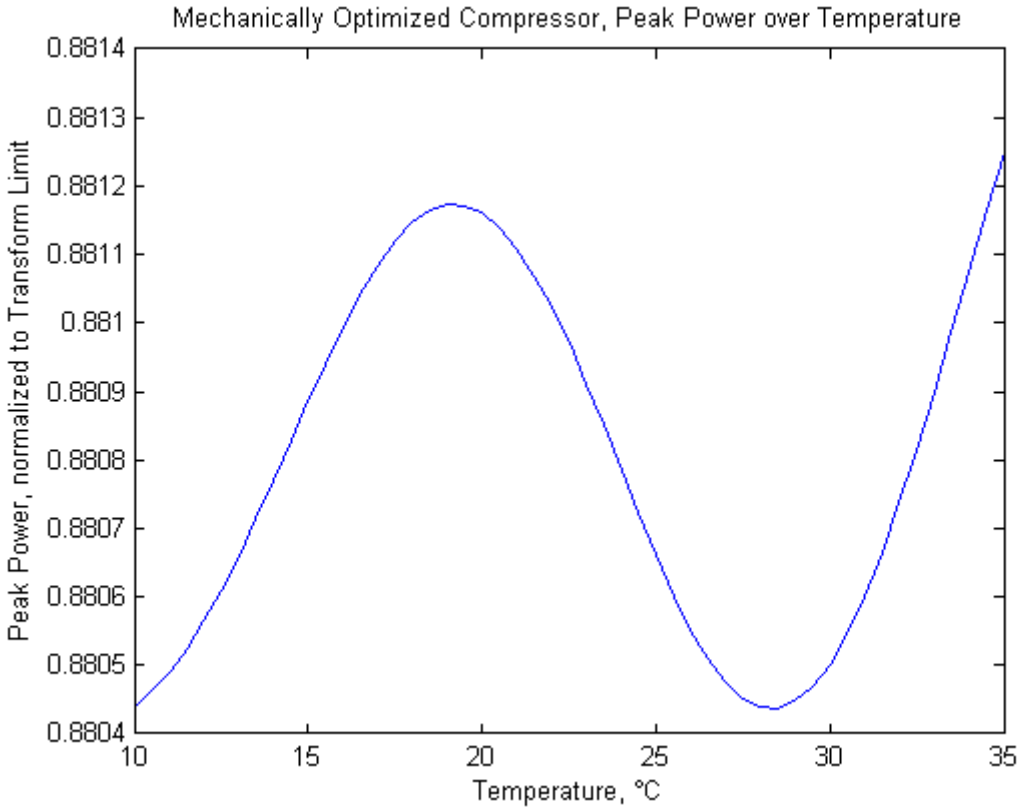


Figure 20. Peak power variation based on temperature dependent refractive index of air.

Much more significant is the dispersion due to the expansion or compression of the mount material of the gratings. Using the well-known value for the coefficient of thermal expansion of aluminum and estimating a mount size of 10 cm, the grating separation changes on the order of 44 μm. This

corresponds to a change in peak power of still less than 1 percent, and is very easily compensated by the DAZZLER. Obviously as these mechanisms are cumulative throughout the system, the cumulative effect of thermal perturbations on the entire system will be an order of magnitude greater than any individual one, but these simulations offer a scale to consider in design.

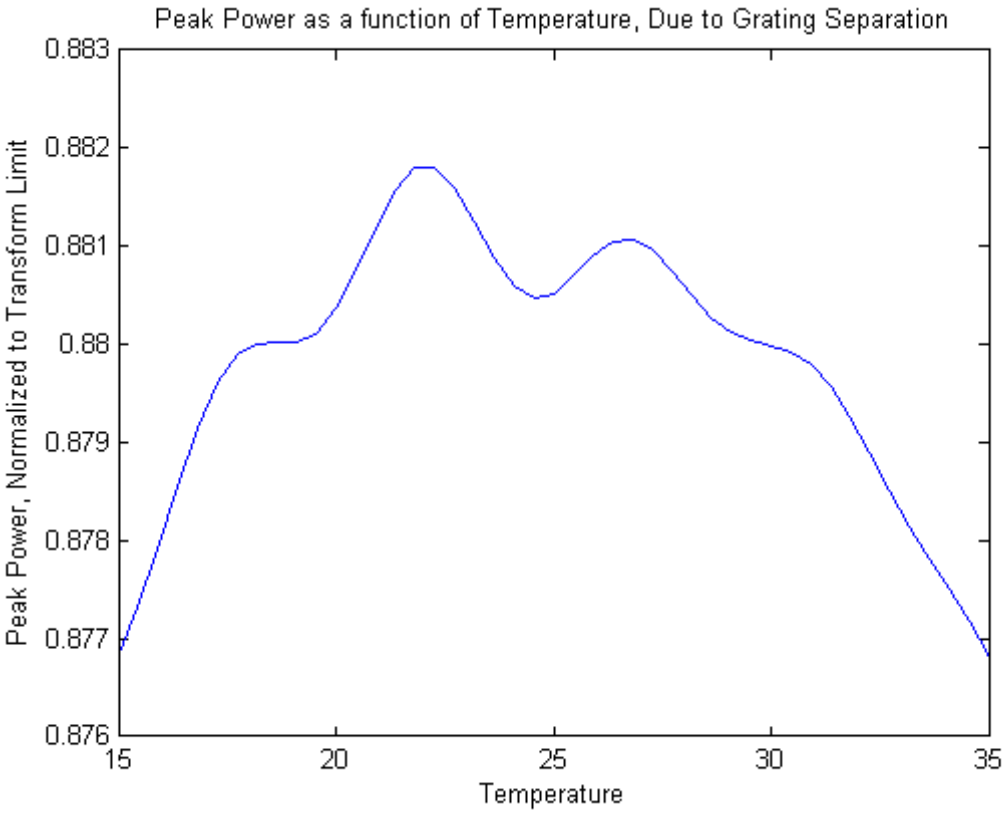


Figure 21. Variation in peak power based on thermal expansion in compressor

## Diagnostics and Feedback

For consistent and robust function of a femtosecond laser, the design must include diagnostics which provide feedback for day-to-day operation and long-term stability. For the front end, pointing stability into the VBG is important to analyze and maintain, as it will have a significant effect on dispersion and amplitude. As this is something that may change relatively easily through slow instability in lens and mirror mounts, it should be monitored constantly; though as it has a very strong effect on spectrum it can be monitored either before or after the regenerative amplifier without much increase in ambiguity. As in a standard Titanium-Sapphire oscillator, it becomes necessary to be able to measure the full pulse characteristics of the oscillator output by way of a frequency resolved optical gate (FROG)[41, 42], as a relatively small change in the oscillator can cause the mode locking mechanism to malfunction or beam pointing to change through the regenerator. That being said, the FemtoFerb fiber oscillator has demonstrated no measureable variation from turn-key performance.

It is critical to have energy measurements and beam profile measurements after each major stage of the laser, to be able to indicate misalignment, damage or associated anomalies (dust spots, color center formation, opto-mechanical variation, pump profile instability etc.). After the compressor, it necessary to characterize the pulse shape and duration, in order to confirm dispersion optimization. To this end, a flip mirror that redirects light into a path toward a characterization section will be implemented, for spectrometer measurements and FROG traces.

## Dispersion Characterization

In order to confirm the function of the VBG, we need a characterization method capable of resolving phase differences generated by delay times on the order of 500 ps. Spectral interferometry is the preferred method, as it is a relatively simple setup with accurate and reproducible results. However, a single shot spectral interferogram with the reference pulse in the center of the chirped pulse, requires a spectrometer with a resolution approaching 1 pm. There are 2 solutions to this problem presented here: First, by scanning the reference pulse over the entire range of the chirped pulse and recording the location of the interferometric against the path delay in time; second, by constructing a spectrometer that can resolve a large portion of the interferogram, and scanning the reference in a few steps over the chirped pulse.

Spectral interferometry is a technique for measuring phase as a function of frequency $\varphi(\omega)$. Two wavefronts are interfered in a Michelson configuration, having the form

$$E_1(\omega) * e^{-i(\Omega(t_1-t_0)+\varphi(\Omega))} ; E_2(\omega) * e^{-i\Omega(t_2-t_0))} \quad (9)$$

Where $\Omega$ is $\omega$-$\omega_0$. Constructive and destructive interference induces an oscillation governed by $i * \Omega * t$ (where $t = t_2 - t_1$). $\varphi(\Delta\omega)$ is the phase added by the CVBG. t is controlled by a translation stage, which will change the path length of the unchirped arm ($t = 2*c*\Delta d$). A spectrometer is used to measure the spectral intensity of the combined beams, and from that data we construct the plot of $\varphi(\Omega)$.

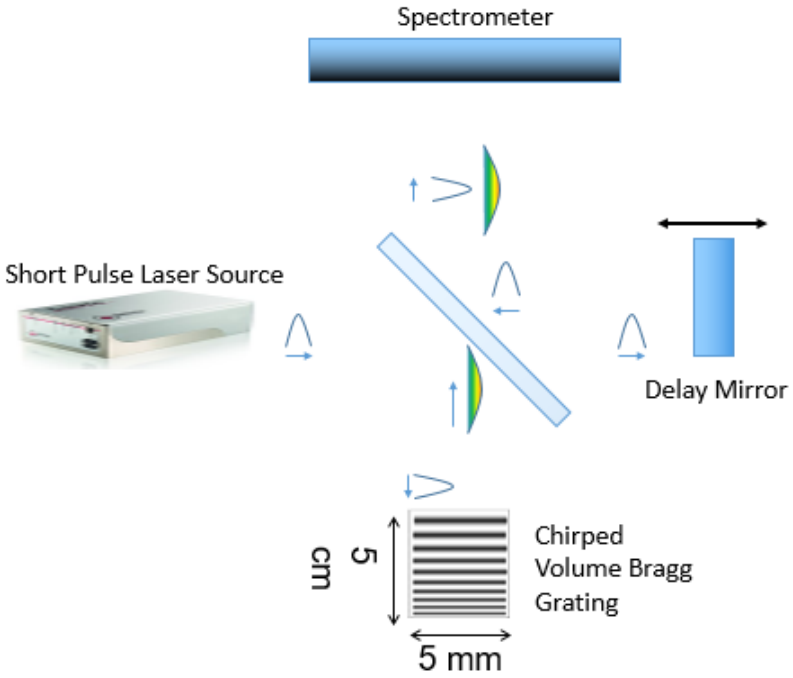


Figure 22. VBG Characterization Setup

$$I = \left|E_1(\omega) + E_2(\omega) * e^{-i\Omega * t - i\varphi(\Omega)}\right|^2 \quad (10)$$

I is the form of the intensity after factoring out a constant phase coefficient, that does not manifest in the intensity measurement. If we are using a 50/50 beam splitter, $E_1$=$E_2$.

$$I = 2E(\omega)^2 + 2E(\omega)^2 * \cos(\Omega * \frac{t}{2} - \frac{\varphi(\Omega)}{2}) \quad (11)$$

The first method does not require a very high resolution spectrometer; it uses a LIBS 2500+ interferometer with 100 pm resolution by Ocean Optics. The recording process is straightforward

and requires almost no post-processing. The slope of peak wavelength vs delay (in time) gives our chirp in ps/nm; a polynomial fit yields the higher orders. As very few cycles are resolved, there is one obvious peak where there is constructive interference. This can be approximated by the convolution of a 100 pm Gaussian over the intensity function. The oscillations that are very fast are averaged out by the relatively broad resolution of the spectrometer.

Often, Taylor expansion of the phase about $\omega_0$ is used to separate orders of phase.

$$\varphi(\omega) = C_1 * (\omega - \omega_0) + \frac{C_2}{2} * (\omega - \omega_0)^2 + \frac{C_3}{6} * (\omega - \omega_0)^3 \quad (12)$$

Where $C_n$ is the $n^{th}$ order of dispersion. This is 3rd order Taylor expansion of $\varphi(\omega)$. $C_1$ is ignored. $C_2$ is the primary variable we are concerned with, as it forms the largest part of the dispersion, followed by $C_3$, which are the 2nd and 3rd derivatives of $\varphi(\omega)$, respectively, usually expressed in $ps^n$.

This is not a very intuitive or immediately useful measurement, as bandwidth is commonly expressed in nm. As such, the equation is transformed slightly to achieve units of ps/nm^(n-1).

$$\frac{1}{2}\frac{d\left(\frac{C_2}{2}*(\Omega)^2+\frac{C_3}{6}*(\Omega)^3-t*\Omega\right)}{d\Omega} \quad (13)$$

$$t = C_2 * (\Omega) + \frac{C_3}{2} * (\Omega)^2 \quad (14)$$

Using the relation

$$\Omega = \omega - \omega_0 = \frac{2*\pi*c}{\lambda} - \frac{2*\pi*c}{\lambda_0} \quad (15)$$

New constants in the wavelength domain can be generated that more intuitively express the linear and quadratic relationship in second and third order dispersion, respectively.

$$D_2 = C_2 * \frac{2*\pi*c}{\lambda_0^2}; D_3 = C_3 * \left(\frac{2*\pi*c}{\lambda_0^2}\right)^2 + C_2 * \frac{2\lambda_0}{2*\pi*c} \quad (16)$$

And our new dispersion equation becomes

$$t = D_2 * (\Delta\lambda) + D_3 * (\Delta\lambda)^2 \quad (17)$$

With $D_2$ and $D_3$ being expressed in ps/nm and ps/nm$^2$ respectively.

Then, Equation 12 becomes

$$t = D_2 * (\Delta\lambda_{peak}) + D_3 * (\Delta\lambda_{peak})^2 \quad (18)$$

making it very easy to fit a 2$^{nd}$ degree polynomial to the plot of t vs. $\Delta\lambda_{peak}$ in order to determine the values for D. Figure 23 shows the peak wavelength near 788 at 55 mm on the translation stage after correcting for the background. This obvious peak is only evident at the wavelength at which

the unchirped pulse coincides with the chirped pulse. 70 or more of these plots are algorithmically processed to show the location of the peak vs time delay.

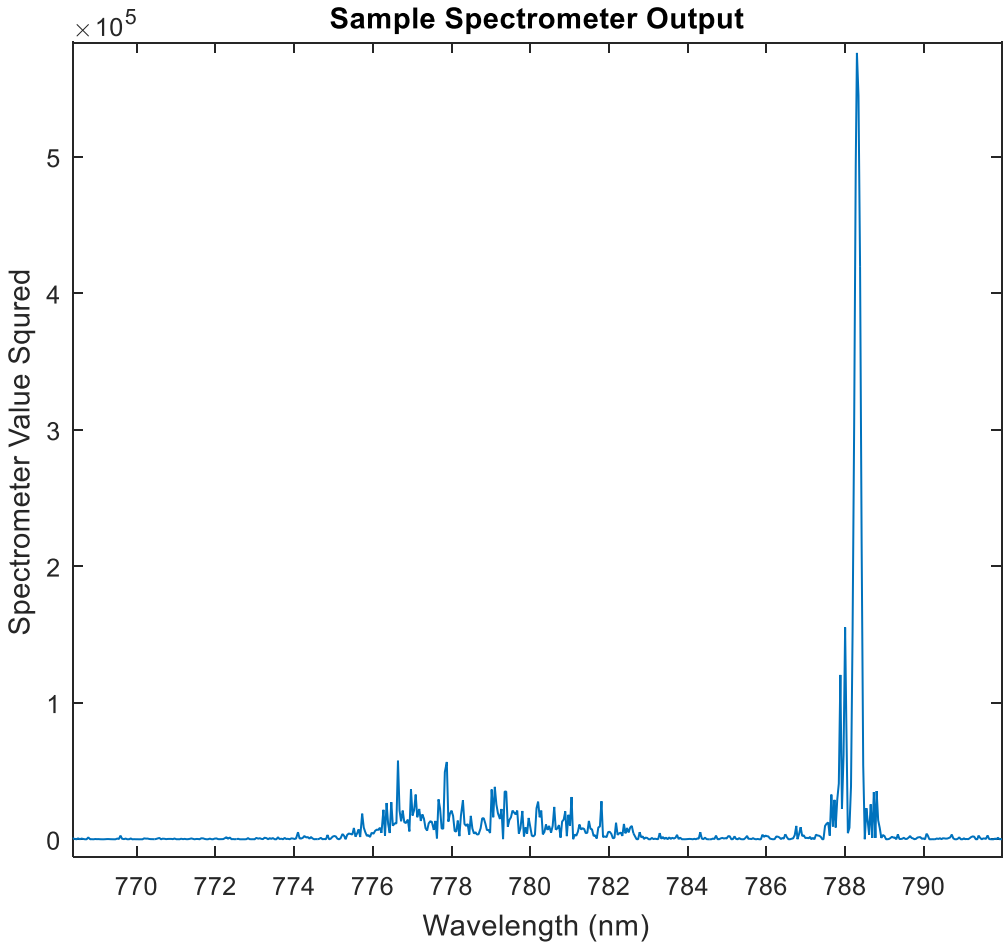


Figure 23. Sample plot of spectral interferometer.

Figure 24 shows one example of the polynomial fit to the custom VBG. The nominal values are $D_3$ = -0.1123 ps/nm$^2$ and $D_2$ = 27.6 ps/nm. The method overall demonstrates roughly +/- 10% confidence on the 3$^{rd}$ order dispersion, which is sufficient for our purposes. Das $\lambda$-$\lambda_0$

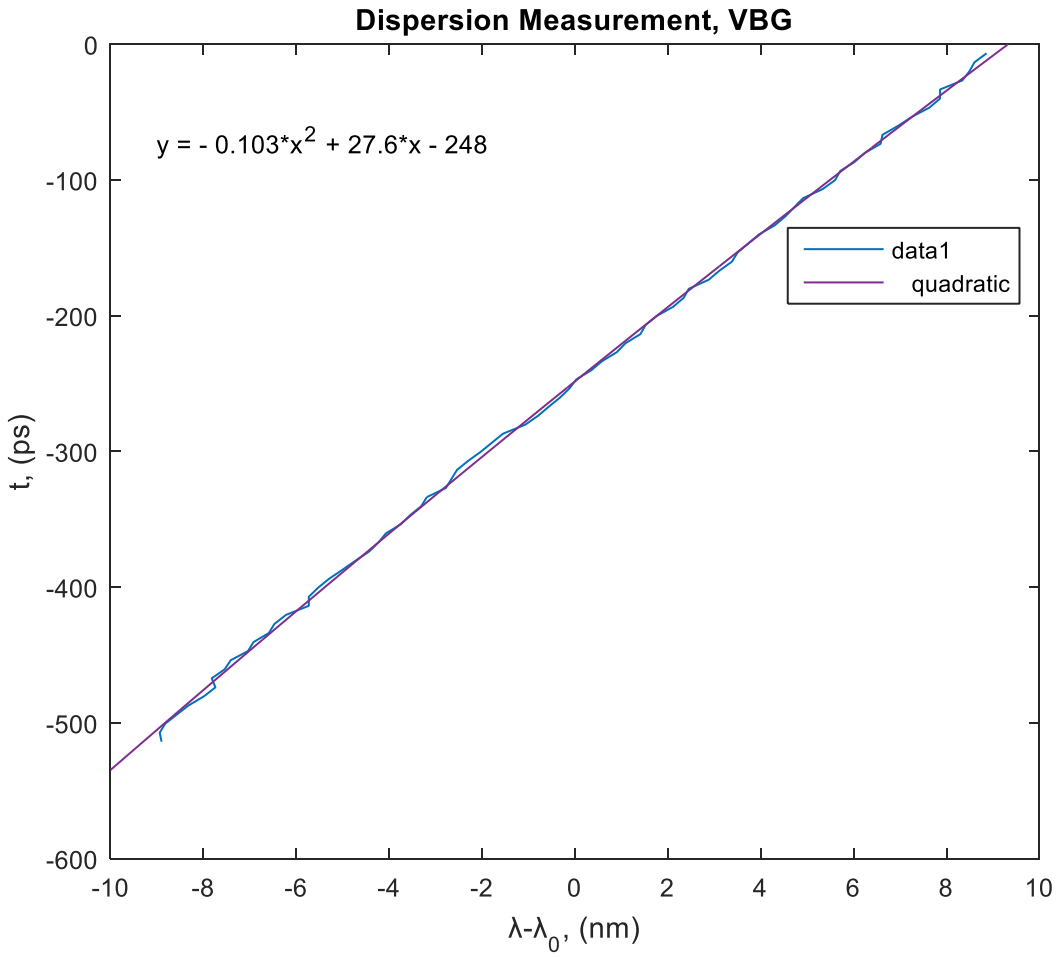


Figure 24. Polynomial fit to custom VBG.

The caveat is that it relies on the position on the translation stage for the measurement of delay. This is subject to inaccuracies due to the angle of the translation stage and the interferometer beam, as well as any imperfections in the screw drive itself. The time delay is extracted directly from the position of the translation, so any angle will appear as faster chirp.

The second method requires the construction of an entire interferometer with several meters of propagation to generate sufficient resolution, but each point in the scan of the reference pulse over the chirped pulse will give information over several nanometers at least. Looking back at Equation 16, the area around the peak is explored within the resolution of the spectrometer. The peak sets the center frequency for the analysis, and about that peak we see oscillations of increasing frequency. Then the relative time delay is adjusted using the translation stage, to a new center, and take the data again; we correct the offset ($t_0$) so that a previously resolved wavelength is at the same delay. As many wavelengths will be resolved redundantly, the technique is self-referencing; the information about phase delay comes from the period of oscillation in the interferogram rather than from the position of the translation stage, eliminating that source of imprecision. As the spectrometer that we constructed also requires rotation scanning of the grating, this method takes more time. It also requires post-processing the data by fitting the oscillation to polynomial cosine function, which is not trivial. In this work, the first characterization method was used.

It is important to simulate the ramifications of small amounts of residual $2^{nd}$ and $3^{rd}$ order dispersion in the output pulse. The VBG is the largest source of dispersion, so it is the largest possible source of uncompensated dispersion. Figure 25 below demonstrate the effects of various

levels of uncompensated 2nd and 3rd order dispersion on the output pulse; it is important to note that optimization using the DAZZLER and compressor adjustment allow for compensation well beyond the uncertainty of the characterization process.

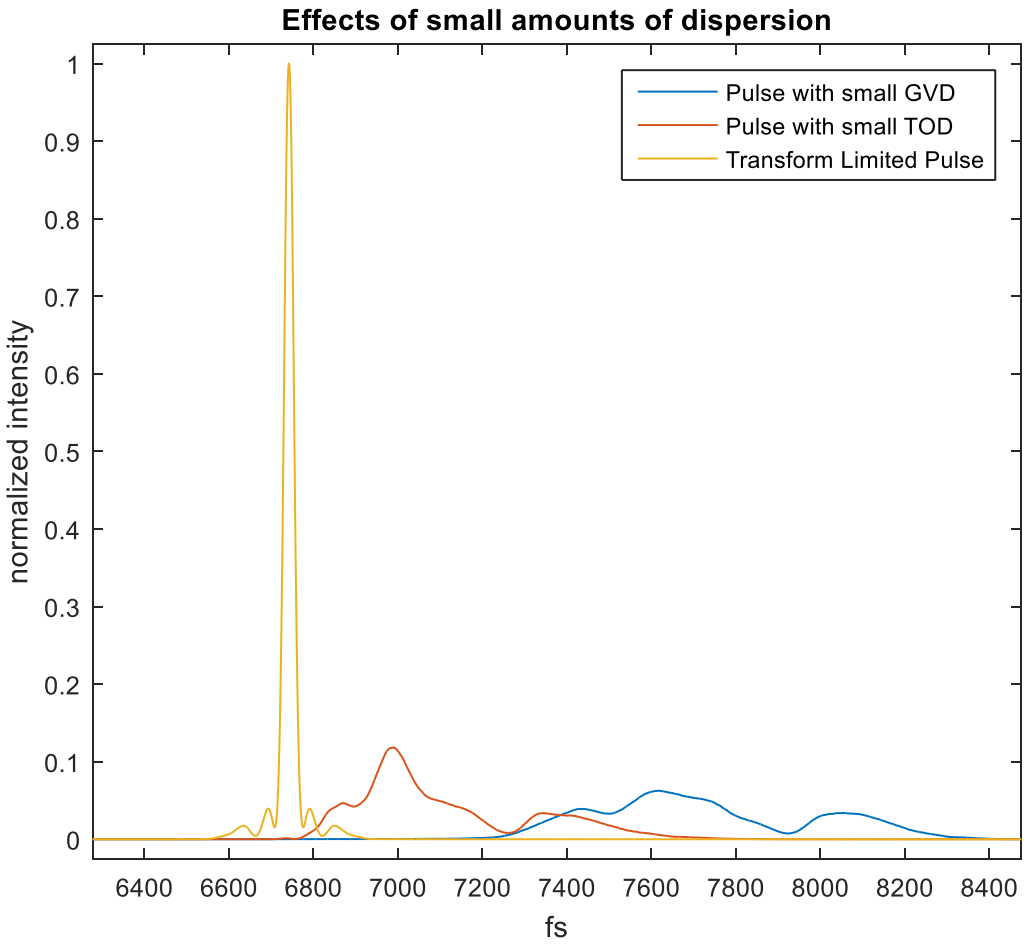


Figure 25. Simulated effects of small amounts of dispersion on TL pulse.

Figure 25 shows the pulse shapes that would be generated if the pulse were chirped with 2nd or 3rd order dispersion equal to 1/1000 of the prescribed stretched value. Depending on the sign of the

chirp, this could lead to slow compensation in air, delaying the onset of the transform limited pulse on the order of 2ps/km. If the residual chirp is positive (the same sign as air) the pulse will continue to broaden as it propagates.

# CONCLUSIONS

In conclusion, the 100 fs 500 mJ MU-HELF laser system was presented. The self-contained laser laboratory will be used in short pulse propagation experiments, with capabilities for beam tracking and dynamic guidance in varied environments, and is in late stage development through the Laser Plasma Laboratory at the University of Central Florida. This system will be the highest energy mobile femtosecond laser system in existence, with several unique innovations that serve to improve long term stability and ease of alignment and diagnostics.

In order provide some background on short pulsed lasers, Chapter 2 presents some methods for generating ultrashort high intensity pulses, including Q switching, Gain Switching, and Mode Locking, alongside a physical description of chirped-pulse amplification. Filamentation, the nonlinear phenomenon that leads to spatial soliton formation in air and a key application for the MU-HELF system is reviewed in some detail as well. In order to generate the short pulse and high energy prescribed, a mode locked oscillator is used to generate a short pulse which then undergoes Chirped-Pulse amplification.

The design of the MU-HELF pairs a chirped VBG stretcher to a Treacy compressor to accomplish CPA. This is believed to be the first implementation of a nonlinear chirped VBG in a high energy CPA system. This requires full characterization of the dispersion of the system so that it can be sufficiently compensated by the VBG. The VBG itself must also be characterized using spectral

interferometry to confirm its performance. The method for measuring very large amounts of dispersion has been confirmed on several sample VBGs before final implementation.

Through the capabilities of the MU-HELF system, the Laser Plasma Laboratory will be capable of unique very long range filament propagation experiments in atmosphere, including dynamic tracking and guidance of illuminated targets up to several kilometers.

# APPENDIX: DISPERSION CHARACTERIZATION MODELING

Figure A1 shows a sample code for calculating dispersion. Φ is the dispersion accumulated over 1mm, or the wave vector k in radians/mm. ω is measured in GHz, and λ is in μm. GDD, TOD, FOD, and FiOD are in $fs^2$, $fs^3$, $fs^4$, and $fs^5$, respectively, and represent accumulation over 1mm of propagation. Calculations were done in Mathematica.

```
% BK7;
lam1 = 0.00600069867;
lam2 = 0.0200179144;
lam3 = 103.560653;
S1 = 1.03961212;
S2 = 0.231792344;
S3 = 1.01046945;
c = 299792458;
λ[ω_] = 2*π*c/ω;
ω0 = 2*π*c/.785;

nBK7[lam_] := ((S1*lam^2/(lam^2 - lam1)) + (S2*lam^2/(lam^2 - lam2)) + (S3*lam^2/(lam^2 - lam3)) + 1)^(1/2);

nBK7[λ_]
```

$$\sqrt{1+\frac{1.01046945`\lambda\_^2}{-103.560653`+\lambda\_^2}+\frac{0.231792344`\lambda\_^2}{-0.0200179144`+\lambda\_^2}+\frac{1.03961212`\lambda\_^2}{-0.00600069867`+\lambda\_^2}}$$

```
ϕ[ω_] := ω*nBK7[λ[ω]]*10^-3/(c*10^6)
Group Delay Dispersion (GDD)
ϕ''[ω0]*10^(30)
46.08585082600593`
Third Order Dispersion (TOD)
ϕ'''[ω0]*10^(30)*10^9
31.6566829513301`
Fourth Order Dispersion (FOD)
ϕ''''[ω0]*10^(30)*10^18
-9.193443715432291`
Fifth Order Dispersion (FiOD)
ϕ'''''[ω0]*10^(30)*10^27
29.578967756162374`
```

Figure A1: Sample code for calculating the material dispersion for BK7.

# REFERENCES


1. Brabec, T. and F. Krausz, *Intense few-cycle laser fields: Frontiers of nonlinear optics.* Reviews of Modern Physics, 2000. **72**(2): p. 545-591.

2. Braun, A., et al., *Self-channeling of high-peak-power femtosecond laser pulses in air.* Optics Letters, 1995. **20**(1): p. 73-75.

3. Rae, S.C. and K. Burnett, *Possible production of cold plasmas through optical-field-induced ionization.* Physical Review A, 1992. **46**(4): p. 2077-2083.

4. Franssen, G.C., et al. *Femtosecond lasers for countermeasure applications*. 2009.

5. Wille, H., et al., *Teramobile: A mobile femtosecond-terawatt laser and detection system*.

6. Kryukov, P.G., *Ultrashort-pulse lasers.* Quantum Electronics, 2001. **31**(2): p. 95.

7. Verdeyen, J.T., *Laser electronics*. 1989: Prentice-Hall International.

8. *THE INVESTIGATION OF PASSIVE LASER QSWITCHING*. 1964, 1964-01-31.

9. Peressini, E.R., *Ruby laser giant-pulse generation by gain-switching.* Applied Physics Letters, 1963. **3**(11): p. 203-205.

10. McClung, F.J. and R.W. Hellwarth, *Giant Optical Pulsations from Ruby.* Applied Optics, 1962. **1**(S1): p. 103-105.

11. Ho, P.T., et al., *Picosecond pulse generation with a cw GaAlAs laser diode.* Applied Physics Letters, 1978. **33**(3): p. 241-242.

12. Lau, K.Y., *Gain switching of semiconductor injection lasers.* Applied Physics Letters, 1988. **52**(4): p. 257-259.

13. Lamb, W.E., *Theory of an Optical Maser.* Physical Review, 1964. **134**(6A): p. A1429-A1450.

14. Hargrove, L.E., R.L. Fork, and M.A. Pollack, *LOCKING OF He–Ne LASER MODES INDUCED BY SYNCHRONOUS INTRACAVITY MODULATION.* Applied Physics Letters, 1964. **5**(1): p. 4-5.

15. Garside, B.K. and T.K. Lim, *Laser mode locking using saturable absorbers.* Journal of Applied Physics, 1973. **44**(5): p. 2335-2342.

16. DeMaria, A.J., D.A. Stetser, and H. Heynau, *SELF MODE-LOCKING OF LASERS WITH SATURABLE ABSORBERS.* Applied Physics Letters, 1966. **8**(7): p. 174-176.

17. Maine, P., et al., *Generation of ultrahigh peak power pulses by chirped pulse amplification.* IEEE Journal of Quantum Electronics, 1988. **24**(2): p. 398-403.

18. Strickland, D. and G. Mourou, *Compression of amplified chirped optical pulses.* Optics Communications, 1985. **55**(6): p. 447-449.

19. Pessot, M., et al., *Chirped-pulse amplification of 100-fsec pulses.* Optics Letters, 1989. **14**(15): p. 797-799.

20. Verluise, F., et al., *Arbitrary dispersion control of ultrashort optical pulses with acoustic waves.* Journal of the Optical Society of America B, 2000. **17**(1): p. 138-145.

21. Tournois, P., *Acousto-optic programmable dispersive filter for adaptive compensation of group delay time dispersion in laser systems.* Optics Communications, 1997. **140**(4): p. 245-249.

22. Sellmeier, W., Ann. Phys. Chem. , 1871. **219**(6): p. 272.

23. Ghosh, G., *Sellmeier coefficients and dispersion of thermo-optic coefficients for some optical glasses.* Applied Optics, 1997. **36**(7): p. 1540-1546.

24. *Preface to the First Edition A2 - Diels, Jean-Claude*, in *Ultrashort Laser Pulse Phenomena (Second Edition)*, W. Rudolph, Editor. 2006, Academic Press: Burlington. p. xvii-xxi.

25. Stuart, B.C., et al., *Optical ablation by high-power short-pulse lasers.* Journal of the Optical Society of America B, 1996. **13**(2): p. 459-468.

26. Chiao, R.Y., E. Garmire, and C.H. Townes, *Self-Trapping of Optical Beams.* Physical Review Letters, 1964. **13**(15): p. 479-482.

27. Couairon, A. and A. Mysyrowicz, *Femtosecond filamentation in transparent media.* Physics Reports, 2007. **441**(2–4): p. 47-189.

28. Deng, Z. and J.H. Eberly, *Multiphoton absorption above ionization threshold by atoms in strong laser fields.* Journal of the Optical Society of America B, 1985. **2**(3): p. 486-493.

29. Chin, S.L., *Femtosecond Laser Filamentation*. 2010: Springer New York.

30. Durand, M., et al., *Kilometer range filamentation.* Optics Express, 2013. **21**(22): p. 26836-26845.

31. Sivan, Y., et al. *Control of the Filamentation Distance and Pattern in Long Range Atmospheric Propagation*. in *Nonlinear Photonics*. 2007. Quebec City: Optical Society of America.

32. Lin, H. and K.Y. Lin, *Passively mode-locked fiber lasers*. 2000, Google Patents.

33. Hill, K.O., *Aperiodic Distributed-Parameter Waveguides for Integrated Optics.* Applied Optics, 1974. **13**(8): p. 1853-1856.

34. Hill, K.O. and G. Meltz, *Fiber Bragg grating technology fundamentals and overview.* Lightwave Technology, Journal of, 1997. **15**(8): p. 1263-1276.

35. Glebov, L., et al., *Volume-chirped Bragg gratings: monolithic components for stretching and compression of ultrashort laser pulses.* Optical Engineering, 2014. **53**(5): p. 051514-051514.

36. Renk, K.F., *Titanium–Sapphire Laser*, in *Basics of Laser Physics*. 2012, Springer. p. 75-80.

37. Zhao, K., et al., *Tailoring a 67 attosecond pulse through advantageous phase-mismatch.* Optics Letters, 2012. **37**(18): p. 3891-3893.

38. Fox, A.J., *Acousto-optic modulator*. 1988, Google Patents.

39. Kaplan, D. and P. Tournois, *Theory and performance of the acousto optic programmable dispersive filter used for femtosecond laser pulse shaping.* J. Phys. IV France, 2002. **12**(5): p. 69-75.

40. Treacy, E., *Optical pulse compression with diffraction gratings.* IEEE Journal of Quantum Electronics, 1969. **5**(9): p. 454-458.

41. Kane, D.J. and R. Trebino, *Characterization of arbitrary femtosecond pulses using frequency-resolved optical gating.* IEEE Journal of Quantum Electronics, 1993. **29**(2): p. 571-579.

42. DeLong, K.W., et al., *Frequency-resolved optical gating with the use of second-harmonic generation.* Journal of the Optical Society of America B, 1994. **11**(11): p. 2206-2215.